

Geophysical Research Letters®

RESEARCH LETTER

10.1029/2021GL097592

Key Points:

- Using the Magnetospheric Multiscale data, we report the first observation of electron cyclotron harmonic (ECH) waves within mirror mode structures in the Earth's outer magnetosphere
- The mirror mode structures observed as quasi-periodic magnetic oscillations are excited by anisotropic ions
- The simultaneously detected ECH waves are excited by the electron mirror loss-cone distributions inside the mirror mode structures

Supporting Information:

Supporting Information may be found in the online version of this article.

Correspondence to:






X. Gao,
gaoxl@mail.ustc.edu.cn

Citation:

Chen, R., Gao, X., Lu, Q., Tsurutani, B. T., Chen, H., & Wang, S. (2022). First observation of electron cyclotron harmonic waves inside mirror mode structures in the Earth's outer magnetosphere. *Geophysical Research Letters*, 49, e2021GL097592. <https://doi.org/10.1029/2021GL097592>

Received 21 DEC 2021
Accepted 11 SEP 2022

First Observation of Electron Cyclotron Harmonic Waves Inside Mirror Mode Structures in the Earth's Outer Magnetosphere

Rui Chen^{1,2} , Xinliang Gao^{1,2} , Quanming Lu^{1,2} , Bruce T. Tsurutani³ , Huayue Chen^{1,2} , and Shui Wang^{1,2}

¹CAS Key Laboratory of Geospace Environment, School of Earth and Space Sciences, University of Science and Technology of China, Hefei, China, ²CAS Center for Excellence in Comparative Planetology, Hefei, China, ³Retired, Pasadena, CA, USA

Abstract Electron cyclotron harmonic (ECH) waves are one of the most common plasma waves in the Earth's magnetosphere, and they are considered to be excited by the electron loss-cone distributions near the magnetic equator. Using the Magnetospheric Multiscale data, we report an unusual event of ECH waves at $L = \sim 12.4$ and MLT = ~ 16.0 hr, where the ECH waves are locally excited inside non-propagating magnetic oscillations, that is, mirror mode structures. The observation reveals that the mirror mode structures are generated by anisotropic ions ($T_{i\perp}/T_{i\parallel} \sim 1.3 - 1.7$), and electron mirror loss-cone distributions are formed due to the magnetic configuration of the mirror mode structures. Combining with the linear instability analysis, we confirm that the ECH waves are locally excited by the electron mirror loss-cone distributions inside the mirror mode structures. Therefore, we propose that the mirror mode structures provide another potential source region for ECH waves in the Earth's magnetosphere.

Plain Language Summary Electron cyclotron harmonic (ECH) waves are widely observed in the Earth's magnetosphere, which are important for the diffusion auroral precipitation. Previous studies have shown that the main source region of ECH waves in the magnetosphere is near the magnetic equator, and the electron loss-cone distribution provides the free energy to excite ECH waves. In this study, we reveal that there also exists another potential source region of ECH waves, that is, mirror mode structures. Using the Magnetospheric Multiscale data, we report an unusual event of ECH waves inside the mirror mode structures in the Earth's outer magnetosphere. By analyzing the plasma conditions, we show that the mirror mode structures are generated by anisotropic ions, and electron mirror loss-cone distributions are formed due to the magnetic configuration of the mirror mode structures. Based on the linear instability analysis, we demonstrate that the ECH waves are excited by the electron mirror loss-cone distributions within the mirror mode structures. These results provide new insights into the generation of ECH waves in the Earth's magnetosphere.

1. Introduction

Electron cyclotron harmonic (ECH) waves, also known as electron Bernstein waves, are electrostatic emissions with multiple bands between harmonics of the electron cyclotron frequency (Kennel et al., 1970; Liu, Chen, & Xia, 2020; Meredith et al., 2009). ECH waves have been reported in the Earth's outer radiation belt (Kennel et al., 1970; Liu, Chen, & Xia, 2020; Meredith et al., 2009), the solar wind (Ma et al., 2021), and the magnetic reconnection region (Li et al., 2020; Yu et al., 2021). ECH waves generally resonate with \sim keV electrons, causing pitch angle scattering to form diffuse aurora at high L-shells ($> \sim 8 R_e$, Horne et al., 2003; Ni et al., 2012). Based on theoretical analyses (Horne et al., 2003; Liu et al., 2018, 2020b), it is generally accepted that ECH waves can be excited by electron loss-cone distributions.

It is widely known that the formation of electron loss-cone distributions at the equator in the magnetosphere is due to the precipitation of electrons within the loss cone into the ionosphere (later called the regular loss cone). At $L = \sim 6$, the regular loss-cone angle is $\sim 3^\circ$ (Horne et al., 2003; Liu et al., 2018). Recent observations have revealed that electrons trapped within mirror mode structures may display a loss-cone distribution but with larger loss-cone angles (Ahmadi et al., 2018; Yao et al., 2018). The loss cone related to the mirror mode structure will be called the mirror loss cone in this study to distinguish it from the regular (equatorially measured) loss cone. The mirror loss-cone distribution can be formed due to the local effect of the evolution of the mirror mode structure in the magnetosheath (Yao et al., 2018).

Mirror mode structures are non-propagating magnetic oscillations (i.e., dips, peaks, or other nearly sinusoidal waveforms) in the rest frame of plasmas (Hasegawa, 1969; Price et al., 1986). Theoretical studies (Crooker & Siscoe, 1977; Hasegawa, 1969; Southwood & Kivelson, 1993) and computer simulations (Price et al., 1986) indicate that high- β (β is the ratio between the plasma thermal pressure and magnetic pressure) anisotropic ions can provide the free energy to generate mirror mode structures. Mirror mode structures have been widely observed in planetary magnetosheaths (Ahmadi et al., 2018; Joy et al., 2006; Tsurutani et al., 1982, 2011), interplanetary space (Enriquez-Rivera et al., 2010; Liu et al., 2006; Russell et al., 2009; Tsurutani et al., 1992), and cometary sheaths (Glassmeier et al., 1993; Russell et al., 1987; Schmid et al., 2014; Tsurutani et al., 1999). Mirror mode structures have also been detected in the Earth's magnetosphere but more rarely (Rae et al., 2007; Soto-Chavez et al., 2019).

In this study, we report the first observation of ECH waves within mirror mode structures in the Earth's outer magnetosphere with the MMS data. In Section 2, we briefly introduce the observation data used in this study. In Section 3, we present the ECH waves correlated with the mirror mode structures in the Earth's outer magnetosphere. Observational results reveal that the mirror mode structures driven by anisotropic ions provide favorable conditions for exciting the ECH waves. This scenario is supported by the linear instability analysis. In Section 4, we summarize and discuss our results.

2. Data Sources

The Magnetospheric Multiscale (MMS) mission consists of four identical satellites, and each satellite carries a number of plasma and field instruments to measure particle distributions and electromagnetic fields (Burch et al., 2016). From July 2015 to February 2016, MMS satellites operated in highly elliptical orbits with perigees of $\sim 1.2 R_E$ and apogees of $\sim 12 R_E$ in GSE coordinates (Fuselier et al., 2016). The orbits remain within $\pm 20^\circ$ of the ecliptic plane. The low-resolution magnetic field with 8 or 16 samples/s (survey mode) is measured by the Fluxgate Magnetometer (Russell et al., 2016). Wave electric (8–120,000 Hz) and magnetic (8–8,000 Hz) power spectra with a cadence of 2 s are provided by the Digital Signal Processor (Le Contel et al., 2016; Lindqvist et al., 2016). The plasma data (such as density and temperature) are obtained from the Fast Plasma Instrument (FPI, Pollock et al., 2016), which measures the velocity-space distributions of electrons and ions from ~ 10 eV to 30 keV.

3. Observation Results

Figure 1 presents an overview of ECH waves observed on 3 September 2015. Figures 1a and 1b show the frequency-time spectrograms of electric and magnetic fields, respectively. Electrostatic waves above $1.0 f_{ce}$ with clear harmonics are identified as ECH waves (Figure 1a). During this time interval, the spacecraft was located in the Earth's outer magnetosphere ($L = \sim 12.4$ and $MLT = \sim 16.0$ hr), which is inferred from the high energy fluxes of ~ 10 keV electrons (Figure 1c) and >10 keV ions (Figure 1d) and low plasma densities ($\sim 1 \text{ cm}^{-3}$; Figure 1e). Figure 1f shows the three components of the magnetic field in GSE coordinates and the total magnetic field. The plasma density is anticorrelated with the magnetic field intensity (Figures 1e and 1f), and the correlation coefficient between the ion (electron) density and the magnetic field is ~ -0.75 (-0.6). There are quasi-periodic magnetic oscillations lasting ~ 3 – 8 min (~ 11 cycles), and the peak of each cycle is marked by a dashed line in Figure 1f. To calculate the velocity of the magnetic structure, we use a timing method following Horbury et al. (2002) based on the relative location of satellites and the time delay for satellites crossing the structures. We first select one magnetic structure (i.e., a peak of the total magnetic field) and determine the temporal and spatial differences of this structure among the four MMS satellites. Then, we use Equation 1 in Horbury et al. (2002) to estimate the structure velocity. The estimated structure velocity in this event is <30 km/s, which is much less than the ion thermal velocity ($\sim 1,000$ km/s). In this event, the ECH waves are observed at different regions within the magnetic oscillation structures (Figures 1a and 1f), that is, near the minimum field regions (B minima, $\sim 11:08$ and $\sim 11:31$ UT) and far away from the B minima ($\sim 11:58$ UT).

The quasi-periodic magnetic oscillations are identified as mirror mode structures based on the observational characteristics. The magnitude of the total magnetic field is repeated in Figure 2a for reference. The plasma β is inversely correlated with the magnitude of the magnetic field and generally larger than 2, even up to ~ 6 in the low magnetic field region (Figure 2a). Here, we use two angles (i.e., θ and φ) to define the direction of the magnetic field. θ is the angle between the magnetic field vector and the z -axis, and φ is the angle between the projection

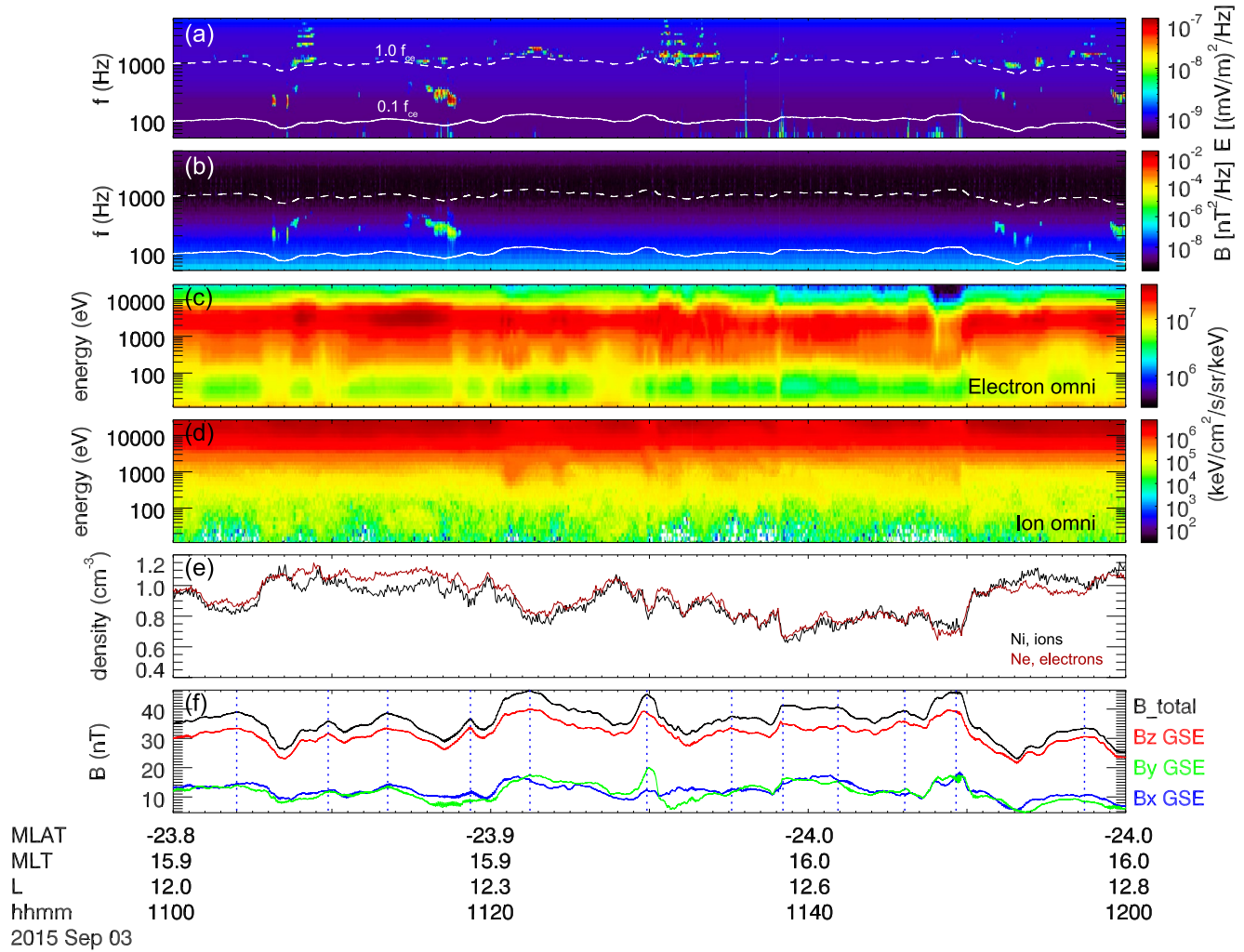


Figure 1. The overview of the observational results during 11:00–12:00 UT, including (a) wave electric spectral density, (b) wave magnetic spectral density, (c) electron energy flux, (d) ion energy flux, (e) ion density (black) and electron density (red), and (f) magnetic field components in GSE coordinate and total magnetic field.

vector (in the x - y plane) and the x -axis. Across the magnetic structures, two magnetic field angles (θ and φ) change less than 10° (Figure 2b), meaning that the direction of the magnetic field changes very slightly. The total pressure (thermal plus magnetic pressure) is nearly constant (Figure 2c). In addition, the magnetic structures are linearly polarized and have large normal angles ($\sim 78^\circ$) relative to the background magnetic field (see Text S1 and Figure S1 in Supporting Information S1). The structure size (the product of the spacecraft velocity and oscillation period; ~ 300 – 760 km) and the magnetic field change (the ratio between the deviation of magnetic magnitude and the average magnetic magnitude during the entire time period; larger than 10%) are consistent with previously reported mirror mode structures (Dimmock et al., 2015; Rae et al., 2007; Tsurutani et al., 1982). In short, these magnetic structures have the following characteristics: (a) quasi-periodic magnetic oscillations, (b) non-propagating in the plasma frame, (c) small magnetic angular changes across the structure, (d) constant total pressure, and (e) linear polarization and large normal angles. All of the above characteristics indicate that those magnetic oscillations are mirror mode structures (Russell et al., 1987; Tsurutani et al., 1982, 2011).

Figure 2d shows that the ions are anisotropic with $T_{i\perp}/T_{i\parallel} \sim 1.3$ – 1.7 ($T_{i\parallel}$ and $T_{i\perp}$ are the parallel and perpendicular components of ion temperature). The threshold for the mirror instability is roughly given by $R = \beta_{i\perp} \left(1 - \frac{T_{i\perp}}{T_{i\parallel}}\right) + 1$ ($\beta_{i\perp} = \frac{n_i k_B T_{i\perp}}{B^2/2\mu_0}$; Hasegawa, 1969), and a negative R means that the criterion of the mirror instability is satisfied. As shown in Figure 2e, the value of R is negative for most of the time and even less than

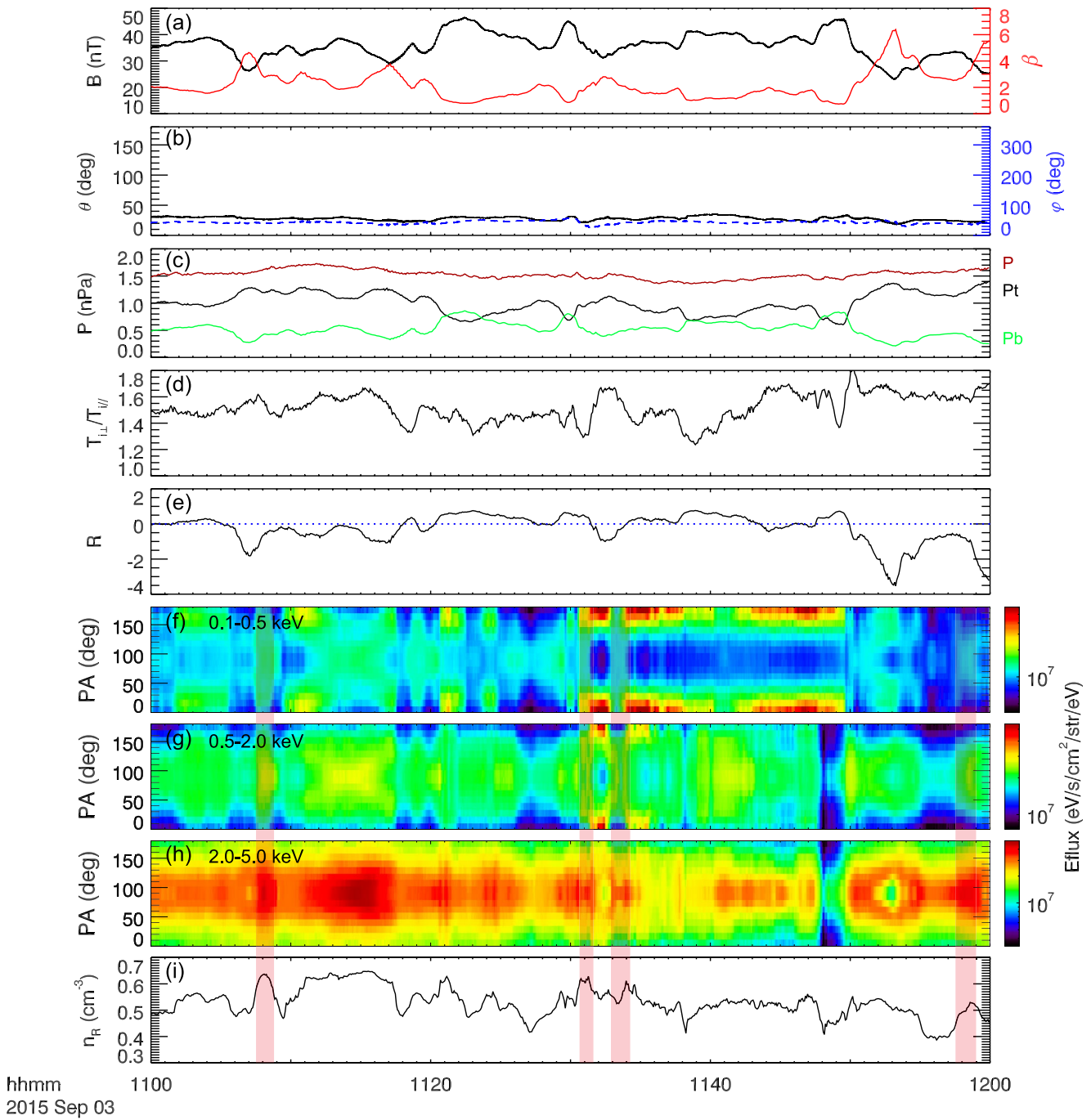


Figure 2. (a) Magnetic field magnitude (black) and plasma β (red), (b) two field angles, (c) magnetic pressure ($P_t = B^2/2\mu_0$, green), thermal pressure ($P_t = n_i T_i$, black) and total pressure (red), (d) ion temperature anisotropy T_{\perp}/T_{\parallel} , and (e) the criterion of mirror instability. (f-h) The pitch angle distribution of energetic electrons in the energy range of 0.1–0.5, 0.5–2.0, and 2.0–5.0 keV, respectively. (i) The number density of resonant electrons with energy ranging from 0.1 to 5.0 keV. In Figures 2d and 2e, the solid and dashed lines represent $0.1 f_{ce}$ (f_{ce} is the local electron cyclotron frequency) and $1.0 f_{ce}$, respectively.

~ 3 (except in several intervals with small positive R values, i.e., $< \sim 0.7$). Theoretically, the mirror mode structures are locally generated by anisotropic ions.

To figure out the generation of ECH waves, the corresponding electron distributions are investigated. Figures 2f–2h show the pitch angle distributions of energetic electrons (0.1–0.5, 0.5–2.0, and 2.0–5.0 keV). The number densities of resonant electrons with energy ranging from 0.1 to 5.0 keV are shown in Figure 2i. Here,

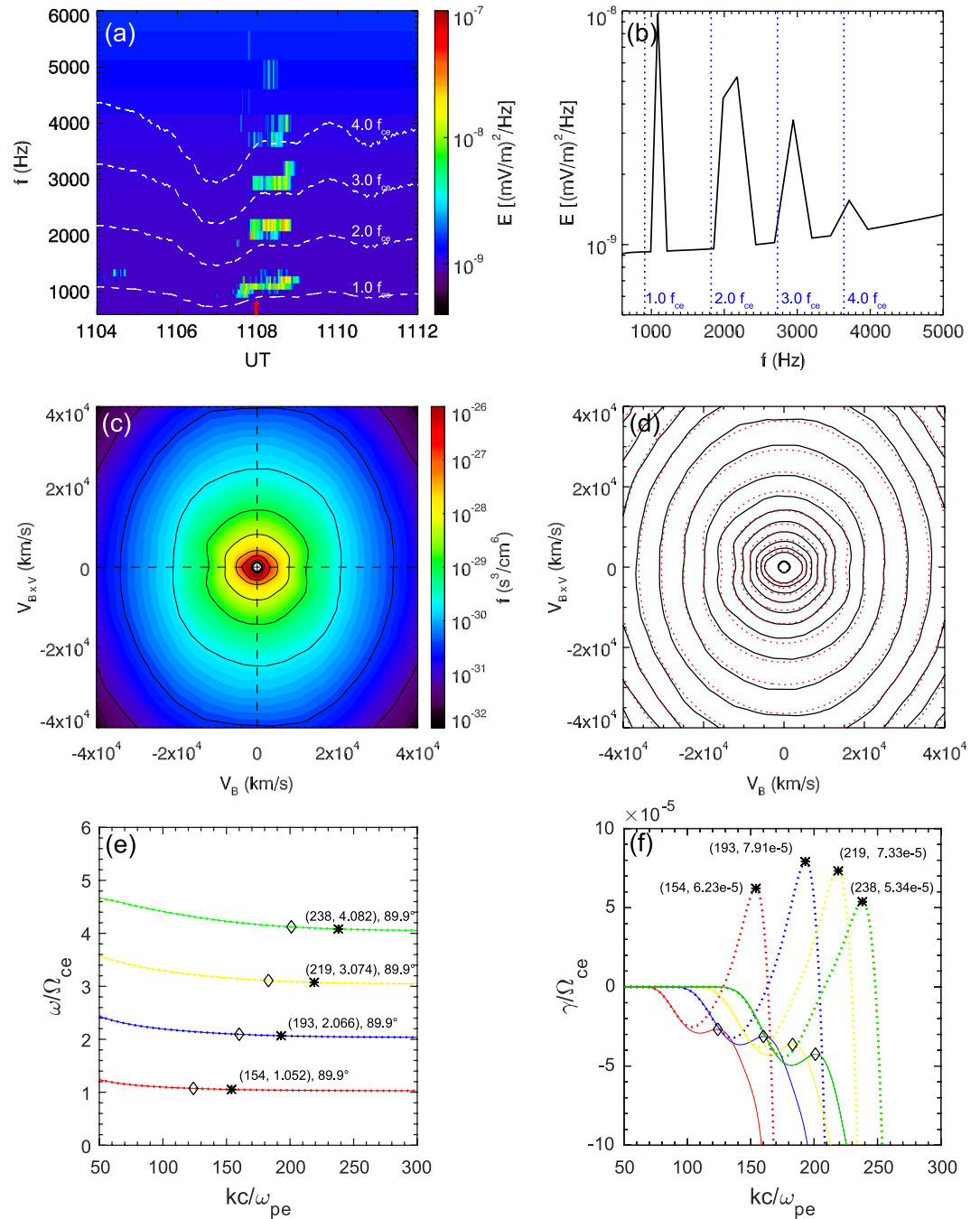


Figure 3. (a) Expanded views of the spectrum at ~11:08 UT in Figure 1a. (b) The profile of the wave electric spectral density at ~11:08 UT marked by the red arrow in Figure 3a as a function of frequency. (c) Electron distribution during the time from 11:07:43 to 11:08:28 UT. (d) The distribution of the electron distribution with its fitted curve. (e) Wave frequency ω/Ω_{ce} and (f) linear growth rate γ/Ω_{ce} as a function of dimensionless wavenumber k at the specific wave normal angle for each harmonic band when both Δ_2 and Δ_3 are set as 0.5 (solid lines) and 0.45 (dashed lines). In Figure 3a, the dashed lines show 1.0 , 2.0 , 3.0 and $4.0 f_{ce}$. In Figures 3c and 3d, V_B (x-axis) represents the velocity along the background magnetic field \vec{B}_0 , and $V_{B \times V}$ (y-axis) represents the velocity along the direction of $\vec{B}_0 \times \vec{V}$ (\vec{V} indicates the bulk velocity). The solid and dashed lines in Figure 3d represent the observed data and their fitted curves, respectively.

the minimum resonant energy of the ECH waves is ~100 eV, which is estimated under the resonant condition ($\omega - k_{\parallel} v_{\parallel} = \Omega_{ce}$) using the parameters from observations (the background magnetic field) and linear theoretical analysis (the wavenumber, frequency, and normal angle, see Figure 3e). While the upper limit of resonant energy is roughly set as 5 keV, since the energy fluxes of >5 keV electrons are much lower (Figure 1c). It is clearly shown

Table 1
The Fitting Parameters for the Electron Distributions in Figures 3d and 4b

	n_e (cm ⁻³)		α_{\parallel} (eV)		α_{\perp} (eV)		Δ		β	
1	0.40	0.30	25	25	18	10	1.0	1.0	0.0	0.0
2	0.35	0.30	120	200	80	120	0.5	0.8	0.4	0.5
3	0.25	0.25	450	650	480	820	0.5	0.7	0.3	0.4
4	0.25	0.10	1,500	1,500	2,200	1,900	1.0	1.0	0.0	0.0

Note. Left black (right red) numbers are the fitting parameters for the electron distribution in Figure 3d (Figure 4b).

that all of these ECH waves (marked by shading regions in Figures 2f–2i) are observed with mirror loss-cone distributions (see Figure 3d, Figure S2a and S2e in Supporting Information S1) and large numbers of resonant electrons (Figure 2i). Other distributions (such as butterfly distributions and beam-like distributions) are also observed inside the structures but are not correlated with ECH waves.

Figure 3a presents an expanded view of the spectrum in Figure 1a. The profile of wave electric spectral densities at ~11:08 UT as a function of frequency is presented in Figure 3b. The frequencies corresponding to the peak power for the four harmonic bands are ~1.21, ~2.31, ~3.24, and ~4.07 f_{ce} , respectively.

Figure 3c shows the simultaneously measured electron velocity distribution inside the mirror mode structure for the ECH waves at ~11:08 UT. The electron velocity distribution is obtained by averaging the fast-mode measurements of FPI (Pollock et al., 2016) from 11:07:43 to 11:08:28 UT. Due to the magnetic mirror configuration, part of the electrons with large pitch angles are trapped and appear as a mirror loss-cone distribution (Figure 3c). To perform the linear instability analysis, we employed the least square method to fit the measured electron velocity distribution by a sum of four subtracted Maxwellian components as $f = \sum_i f_i$, $i = 1-4$ (Horne et al., 2003),

$$f_i = \frac{n_i}{\pi^{3/2} \alpha_{\perp i}^2 \alpha_{\parallel i}} \exp\left(-\frac{v_{\parallel}^2}{\alpha_{\parallel i}^2}\right) \cdot \left[\Delta_i \exp\left(-\frac{v_{\perp}^2}{\alpha_{\perp i}^2}\right) + \frac{1 - \Delta_i}{1 - \beta_i} \cdot \left(\exp\left(-\frac{v_{\perp}^2}{\alpha_{\perp i}^2}\right) - \exp\left(-\frac{v_{\perp}^2}{\beta_i \alpha_{\perp i}^2}\right) \right) \right],$$

where Δ_i and β_i represent the depth and width of the loss cone, thus controlling the shape of the loss-cone distribution. $\alpha_{\parallel i}$ and $\alpha_{\perp i}$ are the parallel and perpendicular thermal velocities relative to the background magnetic field. The number density of each component is represented by n_i . All of the fitting parameters are listed in Table 1. As shown in Figure 3d, the fitted curves (red-dotted lines) are consistent with the measured curves (black lines).

Using the BO model (Xie, 2019), we calculated the dispersion relations and linear growth rates of ECH waves at different wave normal angles (ranging from 88.1° to 89.9° with an interval of 0.2°) to find the theoretical peak linear growth rate for each harmonic band. Figures 3e and 3f show the wave frequency ω/Ω_{ce} and linear growth rate γ/Ω_{ce} as a function of dimensionless wavenumber k at the specific wave normal angle for each harmonic band. The analysis results show that the growth rates are negative based on the fitting parameters (solid lines in Figures 3e and 3f). However, since the excited ECH waves can efficiently scatter energetic electrons to fill the mirror loss cone (Horne et al., 2003; Ni et al., 2012), the measured electron distribution must have relaxed after wave excitation. Therefore, we slightly modify the depth of the observed mirror loss-cone distribution (changing $\Delta_2 = 0.5$ and $\Delta_3 = 0.5$ to $\Delta_2 = 0.45$ and $\Delta_3 = 0.45$) to obtain the possible initial distribution. The results based on the modified distribution are shown as dashed lines in Figures 3e and 3f. The frequencies with the peak growth rate marked by the star for each harmonic band are ~1.052, ~2.066, ~3.074, and ~4.082 f_{ce} , respectively. Both theoretical results are consistent with the observations, considering the low resolution in the high-frequency range (128 Hz at $f = \sim 1,000-2,000$ Hz, 256 Hz at $f = \sim 2,000-4,000$ Hz). We have changed the depth parameters from 0.5 (fitted value) to 0.3 with an interval of 0.05 to perform our theoretical analyses (see Text S2 and Table S1 in Supporting Information S1). With decreasing Δ_2 and Δ_3 (fewer electrons inside the mirror loss cone), the linear growth rates increase from $\sim -10^{-5}$ to 10^{-3} . The wave frequencies corresponding to the peak growth rates change slightly, that is, $<0.15 f_{ce}$ (~ 130 Hz). The same theoretical analysis is also performed for the other two events (at ~11:31 and ~11:58 UT), and the calculations also agree with the observations. These results can be found in Supporting Information S1 (see Text S3 and Figure S2 in Supporting Information S1).

Figure 4 presents a case without ECH waves for comparison. The electron distribution (11:40:03–11:41:01 UT) in Figure 4a shows no obvious mirror loss-cone shape, compared with that in Figure 3c. We still use four subtracted Maxwellian components to fit the electron distribution. Comparing the fitting parameters of the two cases in Table 1, it is evident that the electron distribution without ECH waves has a larger Δ ($\Delta_2 = 0.8$, $\Delta_3 = 0.7$), which quantitatively confirms the absence of the mirror loss-cone distribution. For component #3, the distribution in Figure 4b has a larger temperature anisotropy (~ 1.26) than that (~ 1.07) in Figure 3d. The absence of the mirror loss-cone distribution and larger anisotropy will strongly reduce the growth rate of ECH waves (Liu et al., 2018). We also adjust the depth parameters in the same way (setting $\Delta_2 = 0.8, 0.7, 0.6, 0.5$, and $\Delta_3 = 0.7, 0.6, 0.5, 0.4$) and perform theoretical analyses at different wave normal angles (ranging from 88.1° to 89.9° with an interval

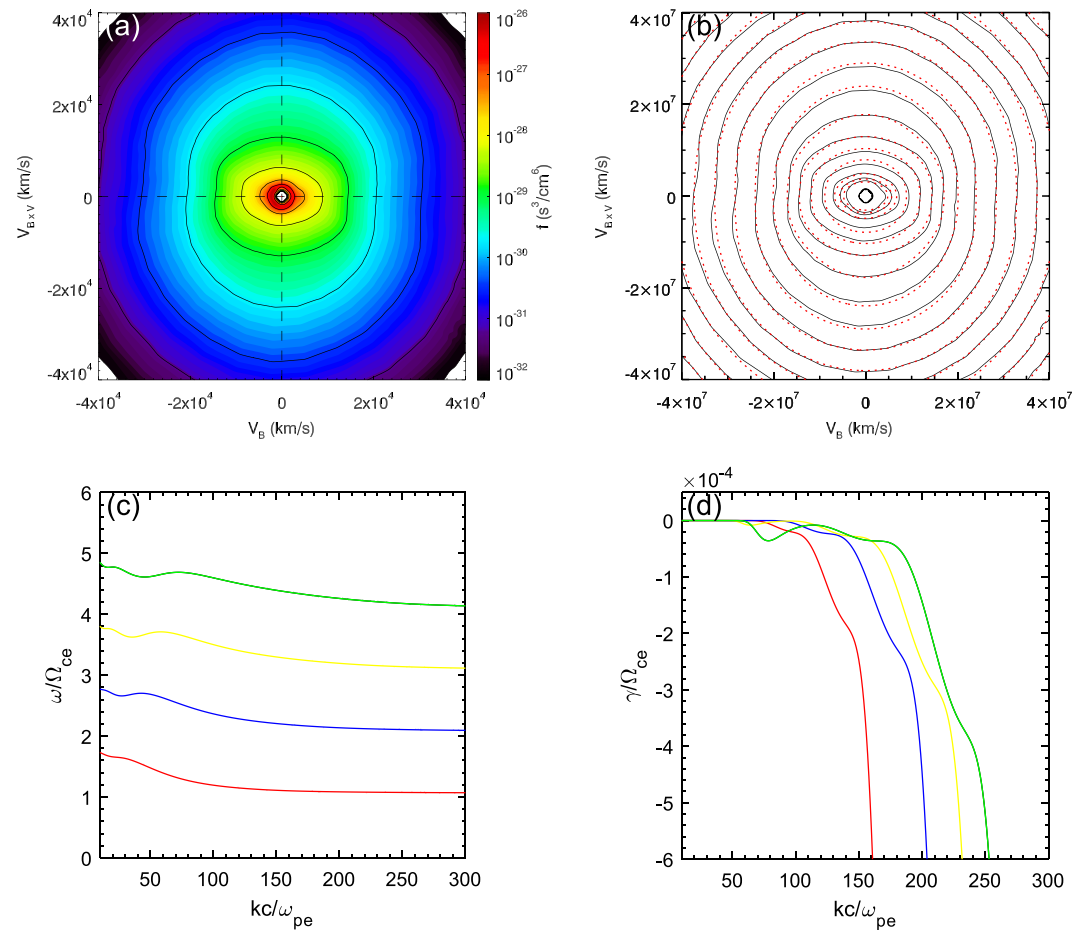


Figure 4. (a) Electron distribution during the time from 11:40:03 to 11:41:01 UT. (b) The distribution with its fitted curve. (c) Wave frequency ω/Ω_{ce} and (d) linear growth rates γ/Ω_{ce} as a function of the dimensionless wavenumber k when the propagation direction θ is set as 89.7° .

of 0.2°) for this case. The linear growth rates of all the calculations remain negative. Figures 4c and 4d show the results when the parameters Δ_2 and Δ_3 are equal to 0.5 and 0.4, respectively. The other calculations with much lower growth rates are not shown.

4. Summary and Discussion

Using the MMS data, we report the first observation of ECH waves inside mirror mode structures in the Earth's outer magnetosphere. The mirror mode structures appear as quasi-periodic magnetic oscillations, and they are excited by anisotropic ions ($T_{i\perp}/T_{i\parallel} > 1$). Due to the configuration of the mirror mode structures, part of electrons with large pitch angles are trapped and have a mirror loss-cone distribution. The linear instability analysis indicates that the ECH waves are generated by the electron mirror loss-cone distributions. Therefore, we propose that the mirror mode structure is a source region for ECH waves in the Earth's magnetosphere.

Observational studies reveal that the low magnetic field magnitude and high plasma density inside the mirror mode structure favor the excitation of whistler-mode waves (named lion roars) in the magnetosheath (Ahmadi et al., 2018; Baumjohann et al., 1999; Smith & Tsurutani, 1976; Tsurutani et al., 1982; Zhang et al., 1998). To our knowledge, this is the first report of ECH waves correlated with mirror mode structures. Part of electrons trapped inside the mirror mode structures typically have a mirror loss-cone distribution. The electron mirror loss-cone distribution is responsible for the generation of ECH waves. Our study has confirmed that the mirror mode structure is a source region for ECH waves in the Earth's magnetosphere. Electron mirror loss-cone distributions are widely observed within magnetosheath's mirror mode structures (Ahmadi et al., 2018; Yao et al., 2018), but there has been

no previous observation of simultaneous ECH waves. It is possible that the plasma β conditions were considerably different for those previous observations. However, this is beyond the scope of the present study.

In this study, we find that the electron mirror loss-cone distribution and the number of resonant electrons are two major factors controlling the generation of ECH waves. All of these ECH waves ($\sim 11:08$, $\sim 11:31$, and $\sim 11:58$ UT) are observed with mirror loss-cone distributions (Figure 3d, Figures S2a and S2e in Supporting Information S1) and a local maximum number of resonant electrons (Figure 2i). When both conditions are satisfied, ECH waves are excited and observed at different regions inside mirror mode structures, that is, near the B minima ($\sim 11:08$ and $\sim 11:31$ UT) and far away from the B minima ($\sim 11:58$ UT). It is worth noting that there also exist some regions with mirror loss-cone distributions and large numbers of resonant electrons but without ECH waves. This may be related to the detailed mirror loss-cone parameters, but it is difficult to understand their contributions based on the presently available data.

Regarding the formation of the electron mirror loss-cone distribution, the formation mechanism remains an open question. Yao et al. (2018) explained it by the local effect of the evolution of mirror-mode structures, which may explain those events observed in the magnetosheath. However, in the magnetosphere, the local effect is insufficient to form such a large loss cone since those electrons between two cone angles (one is the regular loss cone, and the other is the mirror loss cone) cannot be removed. Therefore, other processes (such as cross-field transport, etc.) may lead to the loss of those electrons. Here, both the global and local effects should be taken into consideration, which requires a full study and is beyond the scope of this study. However, electron mirror loss-cone distributions inside mirror-mode structures have been widely observed.

We have slightly adjusted the fitting mirror loss-cone depth to calculate the linear growth rate of ECH waves. The FPI instrument cannot give the precise depth and width due to its limited resolution. The excitation of ECH waves is very fast, and thus the measured electron distribution must have relaxed after wave excitation. Moreover, ECH waves can efficiently scatter energetic electrons to fill the mirror loss cone (Horne et al., 2003; Ni et al., 2012). Because of these factors, we can infer that the initial mirror loss-cone distribution should have a smaller depth than the observed distribution. Therefore, it is reasonable to use the modified one to calculate the linear growth rate of ECH waves.

Data Availability Statement

The MMS data used in this study (field and particle data) are available from the website <https://spdf.gsfc.nasa.gov/pub/data/mms/>. The Space Physics Environment Data Analysis Software (SPEDAS) is available from the website <http://spedas.org>. The electron density under specific energy ranges can be obtained using SPEDAS software. The BO model (available from the website: <https://github.com/hsxie/pdrk>) is used to perform linear theoretical analysis. Moreover, the electron PSD data and the growth rates of ECH waves can also be obtained from <https://doi.org/10.12176/01.99.02090>.

Acknowledgments

This research was funded by the Strategic Priority Research Program of Chinese Academy of Sciences Grant No. XDB41000000, the NSFC grants 41774151 and 41631071, the Key Research Program of Frontier Sciences CAS (QYZDJ-SSW-DQC010), the Fundamental Research Funds for the Central Universities (WK3420000013), and the "USTC Tang Scholar" program. The authors acknowledge all of the MMS instrument teams.

References

- Ahmadi, N., Wilder, F. D., Ergun, R. E., Argall, M., Usanova, M. E., Breuillard, H., et al. (2018). Generation of electron whistler waves at the mirror mode magnetic holes: MMS observations and PIC simulation. *Journal of Geophysical Research: Space Physics*, 123, 6383–6393. <https://doi.org/10.1029/2018JA025452>
- Baumjohann, W., Treumann, R. A., Georgescu, E., Haerendel, G., Fornacon, K.-H., & Auster, U. (1999). Waveform and packet structure of lion roars. *Annales Geophysicae*, 17(12), 1528–1534. <https://doi.org/10.1007/s00585-999-1528-9>
- Burch, J. L., Moore, T. E., Torbert, R. B., & Giles, B. L. (2016). Magnetospheric multiscale overview and science objectives. *Space Science Reviews*, 199(1–4), 5–21. <https://doi.org/10.1007/s11214-015-0164-9>
- Crooker, N. U., & Siscoe, G. L. (1977). A mechanism for pressure anisotropy and mirror instability in the dayside magnetosheath. *Journal of Geophysical Research*, 82(1), 185–186. <https://doi.org/10.1029/JA082i001p00185>
- Dimmock, A. P., Osmane, A., Pulkkinen, T. I., & Nykyri, K. (2015). A statistical study of the dawn-dusk asymmetry of ion temperature anisotropy and mirror mode occurrence in the terrestrial dayside magnetosheath using THEMIS data. *Journal of Geophysical Research: Space Physics*, 120, 5489–5503. <https://doi.org/10.1002/2015JA021192>
- Enriquez-Rivera, O., Blanco-Cano, X., Russell, C. T., Jian, L. K., Luhmann, J. G., Maksimovic, M., et al. (2010). Mirror mode structures in the solar wind: STEREO observations. *AIP Conference Proceedings*, 1216, 276–279. <https://doi.org/10.1063/1.3395854>
- Fuselier, S. A., Lewis, W. S., Schiff, C., Ergun, R., Burch, J. L., Petrinec, S. M., & Trattner, K. J. (2016). Magnetospheric multiscale science mission profile and operations. *Space Science Reviews*, 199(1–4), 77–103. <https://doi.org/10.1007/s11214-014-0087-x>
- Glassmeier, K.-H., Motschmann, U., Mazelle, C., Neubauer, F. M., Sauer, K., Fuselier, S. A., & Acuna, M. H. (1993). Mirror modes and fast magnetoacoustic waves near the magnetic pileup boundary of comet P/Halley. *Journal of Geophysical Research*, 98(A12), 955–964. <https://doi.org/10.1029/93JA02582>

- Hasegawa, A. (1969). Drift mirror instability in the magnetosphere. *Physics of Fluids*, 12, 2642–2650. <https://doi.org/10.1063/1.1692407>
- Horbury, T., Cargill, P., Lucek, E., Eastwood, J., Balogh, A., Dunlop, M., et al. (2002). Four spacecraft measurements of the quasiperpendicular terrestrial bow shock: Orientation and motion. *Journal of Geophysical Research*, 107(A8), SSH10-1–SSH10-11. <https://doi.org/10.1029/2001JA000273>
- Horne, R. B., Thorne, R. M., Meredith, N. P., & Anderson, R. R. (2003). Diffuse auroral electron scattering by electron cyclotron harmonic and whistler mode waves during an isolated substorm. *Journal of Geophysical Research*, 108(A7), 1290. <https://doi.org/10.1029/2002JA009736>
- Joy, S. P., Kivelson, M. G., Walker, R. J., Khurana, K. K., Russell, C. T., & Paterson, W. R. (2006). Mirror-mode structures in the Jovian magnetosheath. *Journal of Geophysical Research*, 111, A12212. <https://doi.org/10.1029/2006JA011985>
- Kennel, C. F., Scarf, F. L., Fredricks, R. W., McGehee, J. H., & Coroniti, F. V. (1970). VLF electric field observations in the magnetosphere. *Journal of Geophysical Research*, 75(31), 6136–6152. <https://doi.org/10.1029/JA075i031p06136>
- Le Contel, O., Leroy, P., Roux, A., Coillot, C., Alison, D., Bouabdellah, A., et al. (2016). The search-coil magnetometer for MMS. *Space Science Reviews*, 199(1–4), 257–282. <https://doi.org/10.1007/s11214-014-0096-9>
- Li, Y., Graham, D. B., Khotyaintsev, Y. V., Vaivads, A., André, M., Min, K., et al. (2020). Electron Bernstein waves driven by electron cresscents near the electron diffusion region. *Nature Communications*, 11(1), 141. <https://doi.org/10.1038/s41467-019-13920-w>
- Lindqvist, P.-A., Olsson, G., Torbert, R. B., King, B., Granoff, M., Rau, D., et al. (2016). The spin-plane double probe electric field instrument for MMS. *Space Science Reviews*, 199(1–4), 137–165. <https://doi.org/10.1007/s11214-014-0116-9>
- Liu, X., Chen, L., Engel, M. A., & Jordanova, V. K. (2020b). Global simulation of electron cyclotron harmonic wave instability in a storm-time magnetosphere. *Geophysical Research Letters*, 47(6), e2019GL086368. <https://doi.org/10.1029/2019GL086368>
- Liu, X., Chen, L., Gu, W., & Zhang, X.-J. (2018). Electron cyclotron harmonic wave instability by loss-cone distribution. *Journal of Geophysical Research: Space Physics*, 123, 9035–9044. <https://doi.org/10.1029/2018JA025925>
- Liu, X., Chen, L., & Xia, Z. (2020). The relation between electron cyclotron harmonic waves and plasmopause: Case and statistical studies. *Geophysical Research Letters*, 47(9), e2020GL087365. <https://doi.org/10.1029/2020GL087365>
- Liu, Y., Richardson, J. D., Belcher, J. W., Kasper, J. C., & Skoug, R. M. (2006). Plasma depletion and mirror waves ahead of interplanetary coronal mass ejections. *Journal of Geophysical Research*, 111, A09108. <https://doi.org/10.1029/2006JA011723>
- Ma, J. Q., Gao, X. L., Yang, Z. W., Tsurutani, B. T., Liu, M. Z., Lu, Q. M., & Wang, S. (2021). Nonlinear wave-wave coupling related to whistler-mode and electron Bernstein waves observed by the Parker Solar Probe. *The Astrophysical Journal*, 918(26), 7. <https://doi.org/10.3847/1538-4357/ac0ef4>
- Meredith, N. P., Horne, R. B., Thorne, R. M., & Anderson, R. R. (2009). Survey of upper band chorus and ECH waves: Implications for the diffuse aurora. *Journal of Geophysical Research*, 114, A07218. <https://doi.org/10.1029/2009JA014230>
- Ni, B., Liang, J., Thorne, R. M., Angelopoulos, V., Horne, R. B., Kubyshkina, M., et al. (2012). Efficient diffuse auroral electron scattering by electrostatic electron cyclotron harmonic waves in the outer magnetosphere: A detailed case study. *Journal of Geophysical Research*, 117, A01218. <https://doi.org/10.1029/2011JA017095>
- Pollock, C., Moore, T., Jacques, A., Burch, J., Gliese, U., Saito, Y., et al. (2016). Fast plasma investigation for magnetospheric multiscale. *Space Science Reviews*, 199(1), 331–406. <https://doi.org/10.1007/s11214-016-0245-4>
- Price, C. P., Swift, D. W., & Lee, L.-C. (1986). Numerical simulation of nonoscillatory mirror waves at the Earth's magnetosheath. *Journal of Geophysical Research*, 91(A1), 101–112. <https://doi.org/10.1029/JA091iA01p00101>
- Rae, I. J., Mann, I. R., Watt, C. E. J., Kistler, L. M., & Baumjohann, W. (2007). Equator-S observations of drift mirror mode waves in the dawnside magnetosphere. *Journal of Geophysical Research*, 112, A11203. <https://doi.org/10.1029/2006JA012064>
- Russell, C. T., Anderson, B. J., Baumjohann, W., Bromund, K. R., Dearborn, D., Fischer, D., et al. (2016). The magnetospheric multiscale magnetometers. *Space Science Reviews*, 199(1–4), 189–256. <https://doi.org/10.1007/s11214-014-0057-3>
- Russell, C. T., Blanco-Cano, X., Jian, L. K., & Luhmann, J. G. (2009). Mirror-mode storms: Stereo observations of protracted generation of small amplitude waves. *Geophysical Research Letters*, 36(5), L05106. <https://doi.org/10.1029/2008GL037113>
- Russell, C. T., Riedler, W., Schwingenschuh, K., & Yeroshenko, Y. (1987). Mirror instability in the magnetosphere of comet Halley. *Geophysical Research Letters*, 14(6), 644–647. <https://doi.org/10.1029/GL014i006p00644>
- Schmid, D., Volwerk, M., Plaschke, F., Vörös, Z., Zhang, T. L., Baumjohann, W., & Narit, Y. (2014). Mirror mode structures near Venus and Comet P/Halley. *Annales Geophysicae*, 32(6), 651–657. <https://doi.org/10.5194/angeo-32-651-2014>
- Smith, E. J., & Tsurutani, B. T. (1976). Magnetosheath lion roars. *Journal of Geophysical Research*, 81(13), 2261–2266. <https://doi.org/10.1029/JA081i013p02261>
- Soto-Chavez, A. R., Lanzerotti, L. J., Manweiler, J. W., Gerrard, A., Cohen, R., Xia, Z., et al. (2019). Observational evidence of the drift-mirror plasma instability in Earth's inner magnetosphere. *Physics of Plasmas*, 26(4), 042110. <https://doi.org/10.1063/1.5083629>
- Southwood, D. J., & Kivelson, M. G. (1993). Mirror instability: 1. Physical mechanism of linear instability. *Journal of Geophysical Research*, 98(A6), 9181. <https://doi.org/10.1029/92JA02837>
- Tsurutani, B. T., Lakhina, G. S., Smith, E. J., Buti, B., Moses, S. L., Coroniti, F. V., et al. (1999). Mirror mode structures and ELF plasma waves in the Giacobini-Zinner magnetosheath. *Nonlinear Processes in Geophysics*, 6(3/4), 229–234. <https://doi.org/10.5194/npg-6-229-1999>
- Tsurutani, B. T., Lakhina, G. S., Verkhoglyadova, O. P., Echer, E., Guarnieri, F. L., Narita, Y., & Constantinescu, D. O. (2011). Magnetosheath and heliosheath mirror mode structures, interplanetary magnetic decreases, and linear magnetic decreases: Differences and distinguishing features. *Journal of Geophysical Research*, 116, A02103. <https://doi.org/10.1029/2010JA015913>
- Tsurutani, B. T., Smith, E. J., Anderson, R. R., Ogilvie, K. W., Scudder, J. D., Baker, D. N., & Bame, S. J. (1982). Lion roars and nonoscillatory drift mirror waves in the magnetosheath. *Journal of Geophysical Research*, 87(A8), 6060–6072. <https://doi.org/10.1029/JA087iA08p06060>
- Tsurutani, B. T., Southwood, D. J., Smith, E. J., & Balogh, A. (1992). Nonlinear magnetosonic waves and mirror mode structures in the March 1991 ULYSSES interplanetary event. *Geophysical Research Letters*, 19(12), 1267–1270. <https://doi.org/10.1029/92GL00782>
- Xie, H. (2019). BO: A unified tool for plasma waves and instabilities analysis. *Computer Physics Communications*, 244, 343–371. <https://doi.org/10.1016/j.cpc.2019.06.014>
- Yao, S. T., Shi, Q. Q., Liu, J., Yao, Z. H., Guo, R. L., Ahmadi, N., et al. (2018). Electron dynamics in magnetosheath mirror-mode structures. *Journal of Geophysical Research: Space Physics*, 123, 5561–5570. <https://doi.org/10.1029/2018JA025607>
- Yu, X., Lu, Q., Wang, R., Gao, X., Sang, L., & Wang, S. (2021). Simultaneous observation of whistler waves and electron cyclotron harmonic waves in the separatrix region of magnetopause reconnection. *Journal of Geophysical Research: Space Physics*, 126, e2021JA029609. <https://doi.org/10.1029/2021JA029609>
- Zhang, Y., Matsumoto, H., & Kojima, H. (1998). Lion roars in the magnetosheath: The Geotail observations. *Journal of Geophysical Research*, 103(A3), 4615–4626. <https://doi.org/10.1029/97JA02519>